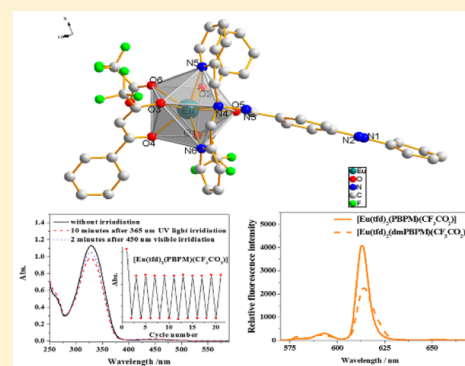


Functionalized Lanthanide(III) Complexes Constructed from Azobenzene Derivative and β -Diketone Ligands: Luminescent, Magnetic, and Reversible Trans-to-Cis Photoisomerization PropertiesLi-Rong Lin,^{*,†} Hui-Hui Tang,[†] Yun-Guang Wang,^{†,‡} Xuan Wang,^{†,‡} Xue-Ming Fang,[†] and Li-Hua Ma^{*,§}[†]Department of Chemistry, College of Chemistry and Chemical Engineering, Xiamen University, Xiamen 361005, People's Republic of China[§]Department of Chemistry, College of Science and Computer Engineering, University of Houston—Clear Lake, 2700 Bay Area Boulevard, Houston, Texas 77058, United States

S Supporting Information

ABSTRACT: The coordination ability of ligands functionalized by azobenzene was manipulated, and two novel chelating ligands, (*E*)-4-(phenyldiazenyl)-*N,N*-bis(pyridin-2-ylmethyl) benzohydrazide (C₂₅H₂₂N₆O, PBPM) and (*E*)-4-((4-(dimethylamino)phenyl)diazenyl)-*N,N*-bis(pyridin-2-ylmethyl) benzohydrazide (C₂₇H₂₇N₇O, dmPBPM), were synthesized. The ligands can offer four coordinating atoms (one oxygen and three nitrogens) to act as tetradentate ligands, together with the two β -diketonates (4,4,4-trifluoro-1-phenylbutane-1,3-dionate, tfd), and the trifluoroacetate anion presented as a ligand and a counterion to form the quaternary units with lanthanide(III) ions (La, Eu, and Gd), [Ln(tfd)₂(PBPM)(CF₃CO₂)₂] (LnC₄₇H₃₄F₉N₆O₇) and [Ln(tfd)₂(dmPBPM)(CF₃CO₂)₂] (LnC₄₉H₃₉F₉N₇O₇), where the lanthanide(III) ions are nine coordinated with N₃O₆ donor sets. All six complexes were structurally characterized, and four crystals were obtained and further analyzed by means of single-crystal X-ray diffraction. They all crystallized in the monoclinic *P*2₁/*c* space group with very similar lattice parameters, forming a monocapped twisted square antiprism. We successfully observed the photoluminescent properties of Eu(III) complexes at a wavelength of 614 nm in both solution and the solid state, as well as the trans-to-cis photoisomerization with the quantum yield ($\Phi_{t \rightarrow c} = 10^{-2}$) of [Eu(tfd)₂(PBPM)(CF₃CO₂)₂] complex that was comparable to that of PBPM. Moreover, the trans-to-cis photoisomerization rates of complexes [Ln(tfd)₂(PBPM)(CF₃CO₂)₂] (La, Eu, Gd) (10^{-3} – 10^{-2} s⁻¹) were also at the same level as that of PBPM and much higher than azobenzene itself (10^{-5} – 10^{-4} s⁻¹). With the aid of TD-DFT calculations, the luminescence of Eu(III) complexes was found to originate from the attenuation effect of β -diketonates. These features provide the foundation for the development of azobenzene-derived β -diketonates lanthanide(III) complexes with photoisomerization and photoluminescence dual functions.



INTRODUCTION

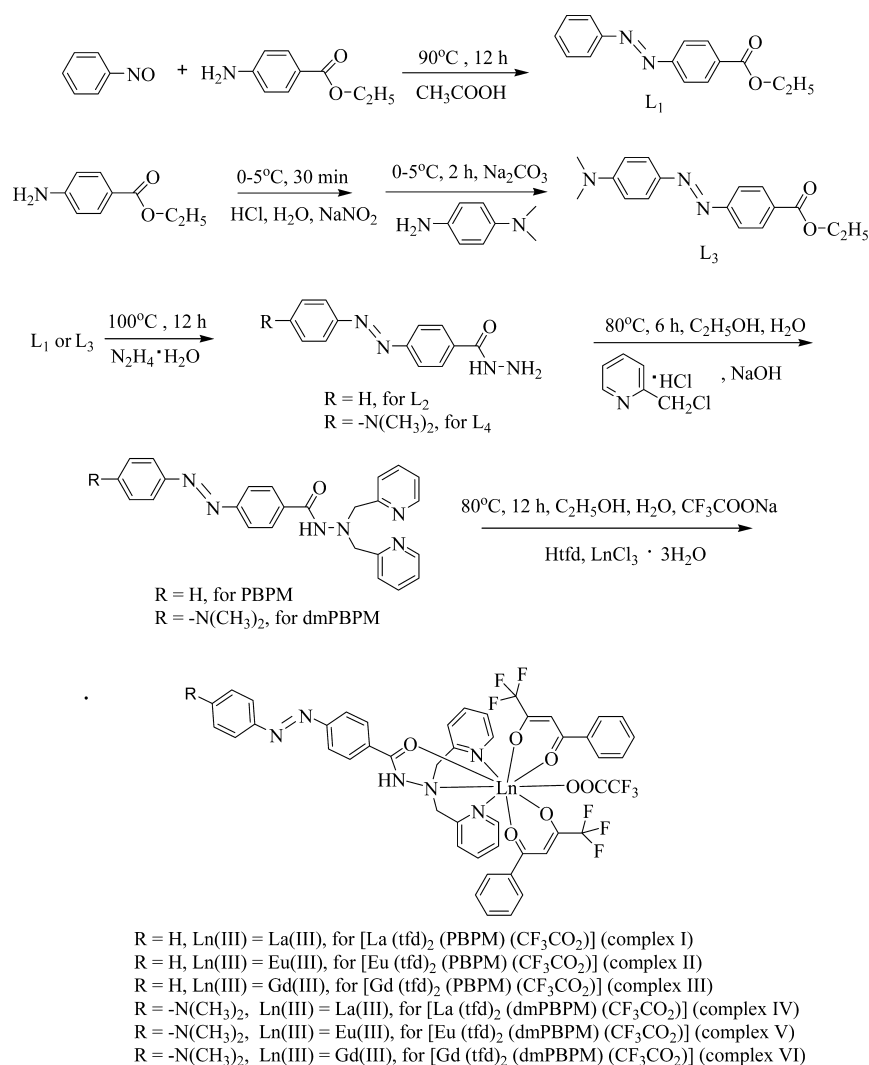
Azobenzene is well known for its trans-to-cis isomerization upon irradiation with UV light, and the reverse isomerization can take place by irradiation with visible light or by heating.¹ A large number of azobenzene derivatives have been studied in solution as well as in polymer matrices.^{2–4} These compounds are promising for application in a wide variety of areas, from biological research to information technology.^{5–9} Azobenzene-functionalized transition metal complexes are an alternative to pure organic azobenzene derivatives and can provide more versatile molecular materials.^{10–12} Combining an azo moiety within coordination compounds can lead to systems capable of exhibiting novel and unusual properties, such as redox, optical, and magnetic properties, of the metal complexes with the photoisomerization reaction. Representative examples are the families of azobenzene-functionalized transition metal complexes that have been studied in detail, such as ferrocene–

azobenzene,^{10,13} bis- or tris(bipyridine),¹⁴ terpyridine metal complexes with azobenzene conjugation,¹⁵ metalladithiolenes with azobenzene groups, and azobenzene-containing tricyclic metalated complexes.^{16,17} Most of the studied complexes displayed trans-to-cis photoisomerization upon UV light and the reverse cis-to-trans isomerization by excitation of the $n-\pi^*$ band of azobenzene.^{18,19} However, the efficiency of the photoisomerization was quite low, and the quantum yields of the trans-to-cis photoisomerization were much lower than those of the organic azobenzenes.²⁰ Some of the metal complexes such as Ir(III) and Ru(II) complexes even showed decreased quantum yields of photoisomerization.^{19,21}

To overcome this difficulty, instead of the d-block group VIII transition metal ions, we focused on the f-block lanthanide ions

Received: November 22, 2016

Scheme 1. Synthetic Procedures Used in the Preparation of PBPM, dmPBPM, and Complexes $[\text{Ln}(\text{tfd})_2(\text{PBPM})(\text{CF}_3\text{CO}_2)]$ and $[\text{Ln}(\text{tfd})_2(\text{dmPBPM})(\text{CF}_3\text{CO}_2)]$



(Ln(III)), a particularly interesting class that possesses unusual electronic properties resulting from shielding of the 4f orbitals by the filled $5s^25p^6$ subshells. Recently, we investigated the photoisomerization properties of a series of azobenzene-derived tris- β -diketonate lanthanide complexes.²² It was found that the presence of Ln(III) enhanced the reversible trans-to-cis isomerization properties of the azobenzene group and increased the fatigue resistance. However, a luminescent property of such azobenzene-derived tris- β -diketonates lanthanide complexes has not been observed at room temperature owing to the forbidden nature of their electronic transitions. The energy could not be transferred from the chromophore to the metal center, which was an obvious drawback for performing useful functions in the fields of fundamental research and possible applications in biological systems and optical data transport.

Combining the information above with the idea to explore the possibility of a luminescent property of azobenzene-derived diketonate lanthanide complexes, we designed and synthesized two new ligands, (*E*)-4-(phenyldiazenyl)-*N,N*-bis(pyridin-2-ylmethyl) benzohydrazide ($\text{C}_{25}\text{H}_{22}\text{N}_6\text{O}$, PBPM) and (*E*)-4-((4-(dimethylamino)phenyl) diazenyl)-*N,N*-bis(pyridin-2-ylmethyl) benzohydrazide ($\text{C}_{27}\text{H}_{27}\text{N}_7\text{O}$, dmPBPM), which are functionalized with an azobenzene group and able to play the

role of a chelating ligand for Ln(III) ions. PBPM or dmPBPM (Scheme 1) consist of an azobenzene moiety, a bis(pyridin-2-ylmethyl)benzohydrazide group, to offer one oxygen and three nitrogen atoms to strongly coordinate with Ln(III) ions. The tetradentate PBPM or dmPBPM ligands, together with two β -diketonates coordinated to the lanthanide center, can form higher coordination number complexes and favor shielding from the solvent molecules.²³ It is well known that the electron-donating substituent groups on the aromatic ring significantly affect the photoisomerization properties of the azo group or photoluminescence of lanthanide(III) complexes.^{1,22,24,25} However, the effect of the electron-donating group on the complexes with photoisomerization and photoluminescence dual functions has barely been reported. We therefore prepared dmPBPM containing the dimethylamino electron-donating group to address the effects of amino N substituents on the photoluminescence and photoisomerization quantum efficiencies of both the free ligand and its Ln(III) complexes and compared their characteristics with those of PBPM. Herein, we present the structural characterization of PBPM and dmPBPM in complexation with the Ln(III) β -diketonates, where 4,4,4-trifluoro-1-phenylbutane-1,3-dionate (tfd) is introduced to the molecular system to construct luminescent Ln(III) β -

diketonates.^{23,26,27} The results reveal the photoluminescent properties of the Eu(III) complexes and the magnetic properties of the Gd(III) complexes as well as an efficient, rapid, reversible, and high quantum yield photoisomerization. We report here the first promising case of an Eu(III) complex with PBPM attached ($[\text{Eu}(\text{tfd})_2(\text{PBPM})(\text{CF}_3\text{CO}_2)_2]$) capable of generating both efficient photoisomerization and impressive photoluminescence. Additionally, easy modification of certain positions of the ligand scaffold would enable the spread of azobenzene-derived ligands and β -diketonate Ln(III) multinary complexes, which will contribute even more to the dual-function materials exploration for applications in the fields of lasers, displays, sensors, solar cells, electroluminescent devices, and biomedical research.

EXPERIMENTAL SECTION

Materials and Methods. $\text{LnCl}_3 \cdot 3\text{H}_2\text{O}$ (Ln = La, Eu and Gd; Jinan Camolai Trading Co.), 4,4,4-trifluoro-1-phenylbutane-1,3-dione (Htfd), ethyl *p*-aminobenzoate and 2-(chloromethyl)pyridine hydrochloride (Leon Technology(Beijing) Co., Ltd.), tetrabutylammonium perchlorate (Adamas Reagent Co., Ltd.), and poly(methyl methacrylate) (PMMA) (Alfa Aesar) were used, and all other chemicals were obtained from Sinopharm Chemicals Group Co. Analytical-grade solvents were redistilled before use. ESI-MS data were acquired on a Bruker ESQUIRE-3000 Plus LC-MS/MS spectrometer. The melting point was determined with an X-4 micromelting point apparatus without correction. Elemental analyses were performed on a Vario EL III elemental analyzer. Solution ^1H NMR spectra were recorded at 400 MHz using a Bruker Advance 400 spectrometer at 25 °C. Chemical shifts (ppm) were determined with TMS as the internal reference. IR spectra (KBr pellets) were recorded on a Nicolet AVATAR FT-IR 330 spectrometer. Thermogravimetric analyses (TGA) were carried out on a SDTQ 600 thermogravimetry under nitrogen atmosphere with a heating rate of 10 °C/min. Absorption spectra were scanned using a Shimadzu UV224012PC absorption spectrometer. The luminescent excitation and emission spectra were recorded using a Hitachi F7000 fluorescence spectrophotometer equipped with a 150 W xenon lamp as excitation source. The maximal wavelength of the Eu(III) complexes is at 614 nm, which is beyond the spectra correction region (less than 600 nm) of this instrument. Therefore, the spectra were uncorrected for detector response, and the slit widths with excitation and emission slits were set at 2.5/5.0 nm. The overall quantum yields of complexes II and V were measured in organic solvent at room temperature, and the emission quantum yield standard was $\text{Ru}(\text{bpy})_2\text{Cl}_2$ in air-saturated aqueous solution ($\Phi = 0.028$).²⁸ Magnetic measurements were carried out at a sweeping rate of 1.5 K min^{-1} on a Quantum Design SQUID XL7 magnetometer in the 2–300 K temperature range. DFT calculations were performed at the three-parametrized Becke–Lee–Yang–Parr (B3LYP) hybrid exchange-correlation functional and 6-31+G(d) basis set using the Gaussian 09 program.²⁹ Low-lying singlet and triplet excitation energies were calculated at the optimized geometries by TD-DFT at the same basis set. The geometries of these compounds were optimized with the DFT(B3LYP) method without considering the solvent effect.

Ligands Syntheses. *Ethyl 4-phenylazobenzoate* (L_1). Nitrosobenzene (0.16 g, 1.5 mmol) was dissolved in glacial acetic acid (6 mL), followed by adding ethyl *p*-aminobenzoate (0.17 g, 1 mmol) and heating to reflux at 90 °C overnight. The resulting solution was cooled to room temperature and poured into water (7 mL). The aqueous solution was extracted three times, each with 20 mL of dichloromethane. The combined organic layers were treated with anhydrous sodium sulfate and filtered. The collected solution was concentrated under reduced pressure and purified by silica gel chromatography with eluting solvent petroleum ether/ethyl acetate (20/1), yielding 0.54 g L_1 (yield 70%) as orange solid: mp 126–127 °C; ESI(+)-MS (m/z , methanol) 254.1 [M^+]; ^1H NMR (400 MHz, CDCl_3) δ ppm = 8.21 (t,

$J = 6.5$ Hz, 2H), 7.97 (d, $J = 8.3$ Hz, 4H), 7.56–7.51 (m, 3H), 4.44 (q, $J = 7.1$ Hz, 2H), 1.45 (t, $J = 7.1$ Hz, 3H).

4-Phenylazobenzohydrazide (L_2). A 0.51 g amount of L_1 compound (2.0 mmol) and 10 mL of hydrazine hydrate (85%) were added into 15 mL of ethanol solution. The solution was refluxed at 100 °C for 12 h under vigorous stirring. A pale yellow solid appeared with time after the mixture was stored in a refrigerator for several hours. The precipitate was filtered and washed with 15 mL of ethanol, 30 mL of cool water, and 15 mL of ethanol, affording a pale yellow solid L_2 0.38 g (yield 79%): mp 146–147 °C; ESI(+)-MS (m/z , methanol) 240.1 [M^+]; ^1H NMR (400 MHz, $\text{DMSO}-d_6$) δ ppm = 9.99 (s, 1H), 8.06–8.01 (m, 2H), 7.96–7.90 (m, 4H), 7.65–7.58 (m, 3H), 4.70 (s, 2H).

(E)-4-(Phenyldiazenyl)-N,N-bis(pyridin-2-ylmethyl) Benzohydrazide (PBPM). 2-Picolyl chloride hydrochloride (0.49 g, 3 mmol) and compound L_2 (0.24 g, 1 mmol) were dissolved in 30 mL of 1:1 ethanol/water and heated to 80 °C. To this solution, 6 mL of aqueous NaOH (1.0 mmol/L) was added dropwise over a period of 30 min, and the resulting solution was additionally stirred for 6 h. The solution was cooled to room temperature, and an orange yellow solid product appeared, which was filtered and washed with mixed water/ethanol (1:1) solvents and then recrystallized from dichloromethane/petroleum ether (1:1) to yield orange PBPM, 0.49 g (yield 58%); mp 151 °C; ESI(+)-MS (m/z , methanol) 445.1 [$M + \text{Na}^+$]; ^1H NMR (400 MHz, $\text{DMSO}-d_6$) δ ppm = 9.82 (s, 1H), 8.48 (s, 2H), 7.93–7.86 (m, 4H), 7.81 (d, $J = 22.2$ Hz, 6H), 7.61 (s, 3H), 7.25 (s, 2H), 4.31 (s, 4H). FT-IR (KBr, cm^{-1}): 3433 (s, O–H), 1654 (s, C=O), 1591 (m, C=C), 1569 (m, N–H), 1477 (s, N=N), 1291 (s, C–N), 855, 820, 768 (m, Ph–H). Anal. Calcd for $\text{C}_{25}\text{H}_{22}\text{N}_6\text{O}$: C, 71.07; H, 5.25; N, 19.89. Found: C, 70.86; H, 5.21; N, 19.82.

Ethyl 4-(4-Dimethylamino)phenylazobenzoate (L_3). Ethyl 4-aminobenzoate (0.83 g, 5.0 mmol) was dissolved in HCl solution (12.0 mL, 3.0 $\text{mol}\cdot\text{L}^{-1}$). A solution of sodium nitrite (0.38 g, 5.5 mmol) in distilled water (12.0 mL) was prepared in a test tube and added dropwise to the acidic solution of ethyl 4-aminobenzoate over 5 min at 0 °C. The mixture was stirred at 0 °C for 30 min. *N,N*-Dimethylaniline (0.61 g, 5.0 mmol) was dissolved in 5 mL of ethanol and cooled to 0 °C, which was added slowly to the above aryldiazonium salt solution at 0 °C. The pH of the resultant colored mixture was adjusted by saturated sodium carbonate solution. After the pH reaching 7–8, the solution immediately turned red, and in a few seconds a red crystalline precipitate of the azo compound was formed. The solution was kept stirring for another 2 h at 0 °C. The precipitate was collected by filtration and washed with water/ethanol (1:1), which was recrystallized from dichloromethane/petroleum ether (1:1) to yield the red compound L_3 , 1.262 g (yield 85%); mp 153–154 °C; ESI(+)-MS (m/z , methanol) 297.2 [M^+]; ^1H NMR (400 MHz, CDCl_3) δ ppm = 8.16 (d, $J = 8.4$ Hz, 2H), 7.91 (dd, $J = 19.0, 8.6$ Hz, 4H), 6.78 (d, $J = 9.0$ Hz, 2H), 4.42 (q, $J = 7.1$ Hz, 2H), 3.13 (s, 6H), 1.44 (t, $J = 7.1$ Hz, 3H).

4-(4-Dimethylamino)phenylazobenzohydrazide (L_4). Hydrazine hydrate (85%, 15 mL) and compound L_3 (0.60 g, 2 mmol) were mixed and refluxed for 12 h under vigorous stirring. After the mixture was kept in a refrigerator for several hours, the yellow solid product appeared, which was filtered and washed with 50 mL of water/ethanol (1:1) mixed solvent precooled on ice, generating compound L_4 , 0.369 g (yield 65%); mp 146–147 °C; ESI(+)-MS (m/z , methanol) 283.1 [M^+]; ^1H NMR (400 MHz, $\text{DMSO}-d_6$) δ ppm = 9.87 (s, 1H), 7.96 (d, $J = 8.5$ Hz, 2H), 7.81 (dd, $J = 8.8, 5.7$ Hz, 4H), 6.84 (d, $J = 9.2$ Hz, 2H), 4.55 (s, 2H), 3.07 (s, 6H).

(E)-4-((4-Dimethylamino)phenyl)diazenyl)-N,N-bis(pyridin-2-ylmethyl) Benzohydrazide (dmPBPM). 2-(Chloromethyl)pyridine hydrochloride (0.10 g, 6 mmol) and compound L_3 (0.57 g, 2 mmol) were dissolved in 15 mL of absolute ethanol and heated to 78 °C. To this solution, 6 mL of 1.0 mmol/L NaOH aqueous solution was added dropwise over a period of 30 min, and the resulting mixture was stirred for an additional 6 h. The forming orange red precipitate was filtered while still hot. The product was washed with water/ethanol (1:1) and then recrystallized from 1:1 dichloromethane/petroleum ether to yield compound dmPBPM as a red solid, 0.065 g

Table 1. Crystallographic Data for Complexes [La(tfd)₂(PBPM)(CF₃CO₂)] (I), [Eu(tfd)₂(PBPM)(CF₃CO₂)] (II), [La(tfd)₂(dmPBPM)(CF₃CO₂)] (IV), and [Gd(tfd)₂(dmPBPM)(CF₃CO₂)] (VI)

crystal data	I	II	IV	VI
CCDC number	1437962	1437960	1437963	1437961
empirical formula	C ₄₇ H ₃₄ F ₉ LaN ₆ O ₇	C ₄₇ H ₃₄ F ₉ EuN ₆ O ₇	C ₄₉ H ₃₉ F ₉ LaN ₇ O ₇	C ₄₉ H ₃₉ F ₉ GdN ₇ O ₇
fw	1104.71	1117.76	1147.78	1167.13
temp (K)	203(2)	203(2)	203(2)	203(2)
wavelength (Å)	0.71073	0.71073	0.71073	0.71073
cryst syst	monoclinic	monoclinic	monoclinic	monoclinic
space group	P2 ₁ /c	P2 ₁ /c	P2 ₁ /c	P2 ₁ /c
a (Å)	24.515(5)	24.109(7)	25.981(1)	25.785(5)
b (Å)	9.862 (2)	9.717(3)	9.741(4)	9.695(2)
c (Å)	19.371(4)	19.229(5)	19.625(7)	19.500(3)
α (deg)	90	90	90	90
β (deg)	101.521(3)	102.483(5)	95.271(1)	96.132(4)
γ (deg)	90	90	90	90
V (Å ³)	4589.0(15)	4398.0(2)	4945.8(3)	4846.8(15)
Z	4	4	4	4
calcd density (Mg m ⁻³)	1.599	1.688	1.541	1.599
abs coeff (mm ⁻¹)	1.026	1.525	0.956	1.462
θ range	3.39–52.00	3.46–51.00	6.01–51.00	3.17–52.00
no. of reflns collected	24 537	22 957	38 361	26 112
data/restraints/parameters	8985/0/631	8188/0/631	9156/0/661	9470/0/660
goodness of fit on F ²	1.144	0.906	1.072	1.149
final R indexes [I ≥ 2σ(I)]	R ₁ = 0.0619 wR ₂ = 0.1299	R ₁ = 0.0414 wR ₂ = 0.0964	R ₁ = 0.0495 wR ₂ = 0.1104	R ₁ = 0.0827 wR ₂ = 0.1484
R indexes [all data]	R ₁ = 0.0725 wR ₂ = 0.1357	R ₁ = 0.0632 wR ₂ = 0.1023	R ₁ = 0.0950 wR ₂ = 0.1404	R ₁ = 0.1257 wR ₂ = 0.1648

(yield 70%); mp 196–197 °C; ESI(+)-MS (*m/z*, methanol) 465.1 [M⁺]; ¹H NMR (400 MHz, CDCl₃) δ ppm = 9.48 (s, 1H), 8.60 (s, 2H), 7.98–7.85 (m, 6H), 7.77 (t, *J* = 7.4 Hz, 2H), 7.67 (d, *J* = 7.5 Hz, 2H), 7.26 (s, 2H), 6.81 (d, *J* = 8.4 Hz, 2H), 4.40 (s, 4H), 3.16 (s, 6H). FT-IR (KBr, cm⁻¹): 3433 (s, O–H), 2923 (m, C–H), 1687 (w, C=C), 1603 (m, C=C), 1547 (m, N–H), 1518 (s, N=N), 1367, 1140 (s, C–N), 858, 820, 767 (m, Ph–H). Anal. Calcd for C₂₇H₂₇N₇O₇: C, 69.66; H, 5.85; N, 21.06. Found: C, 69.10; H, 5.84; N, 21.29.

Synthesis of Lanthanide(III) Complexes. General Procedures. All six complexes were synthesized by the same method described as follows. PBPM (or dmPBPM) (0.25 mmol) and 4,4,4-trifluoro-1-phenylbutane-1, 3-dione (Htfd, 0.162 g, 0.75 mmol) were added to 15 mL of absolute ethanol. The reaction mixture was stirred and heated to 78 °C. To this solution 0.75 mL of 1.0 mmol/L CF₃COONa aqueous solution was added dropwise in 10 min. Then 0.25 mmol of LnCl₃·3H₂O in 5 mL of deionized water was added dropwise, and the resulting mixture was stirred for an additional 10 h at 78 °C. The precipitate appeared after cooling. The crude product was filtered and washed with 30 mL of 1:1 water/ethanol several times and then dried under reduced pressure to give pure solid powder. Crystals of complexes suitable for X-ray analysis were obtained by slow evaporation from their DMF and ethanol mixed solution for about 1 month.

[La(tfd)₂(PBPM)(CF₃CO₂)] (I). Orange solid (0.27 g, yield 83%); mp 180–182 °C; ESI(+)-MS (*m/z*, methanol) 991.4 [M⁺]; ¹H NMR (400 MHz, DMSO-*d*₆) δ ppm = 9.86 (s, 1H), 8.49 (s, 2H), 7.91 (dd, *J* = 18.1, 8.6 Hz, 7H), 7.83–7.72 (m, 6H), 7.64–7.37 (m, 10H), 7.26 (s, 2H), 6.34 (s, 2H), 4.32 (s, 4H). FT-IR (KBr, cm⁻¹): 3433 (s, O–H), 1682 (m, C=O), 1627 (m, C=C), 1577 (m, N–H), 1536 (s, N=N), 1384, 1131 (s, C–N), 1286, 1185 (s, C–F), 819, 795, 761, 629 (m, Ph–H). Anal. Calcd for LaC₄₇H₃₄F₉N₆O₇: C, 51.10; H, 3.10; N, 7.61. Found: C, 50.76; H, 3.08; N, 7.62.

Eu(tfd)₂(PBPM)(CF₃CO₂) (II). Orange solid (0.26 g, yield 87%); mp 198–200 °C; ESI(+)-MS (*m/z*, methanol) 1005.2 [M⁺]; ¹H NMR (400 MHz, DMSO-*d*₆) δ ppm = 9.83 (s, 1H), 8.48 (s, 2H), 7.94–7.72 (m, 10H), 7.60 (s, 3H), 7.30–6.97 (m, 9H), 6.58 (s, 3H), 4.46–4.15 (m, 6H). FT-IR (KBr, cm⁻¹): 3444 (s, O–H), 1687 (m, C=O), 1629

(s, C=C), 1577 (m, N–H), 1538 (s, N=N), 1384, 1132 (s, C–N), 1287, 1185 (s, C–F), 858, 789, 761 (m, Ph–H). Anal. Calcd for EuC₄₇H₃₄F₉N₆O₇: C, 50.50; H, 3.07; N, 7.52. Found: C, 50.55; H, 3.07; N, 7.87.

Gd(tfd)₂(PBPM)(CF₃CO₂) (III). Orange solid (0.26 g, yield 78%); mp 260–262 °C; ESI(+)-MS (*m/z*, methanol) 1010.2 [M⁺]. FT-IR (KBr, cm⁻¹): 3441 (s, O–H), 1687 (s, C=O), 1630 (s, C=C), 1578 (m, N–H), 1537 (s, N=N), 1384, 1132 (s, C–N), 1286, 1185 (s, C–F), 876, 828, 798, 761 (m, Ph–H). Anal. Calcd for GdC₄₇H₃₄F₉N₆O₇: C, 50.27; H, 3.05; N, 7.48. Found: C, 50.20; H, 3.01; N, 7.34.

La(tfd)₂(dmPBPM)(CF₃CO₂) (IV). Dark red solid (0.30 g, yield 87%); mp 243–244 °C; ESI(+)-MS (*m/z*, methanol) 1034.6 [M⁺]; ¹H NMR (400 MHz, DMSO-*d*₆) δ ppm = 9.81 (s, 1H), 8.50 (s, 2H), 7.93 (d, *J* = 7.4 Hz, 4H), 7.82–7.65 (m, 10H), 7.48 (d, *J* = 40.9 Hz, 6H), 7.26 (s, 2H), 6.83 (d, *J* = 9.2 Hz, 2H), 6.34 (s, 2H), 4.32 (s, 4H), 3.07 (s, 6H). FT-IR (KBr, cm⁻¹): 3433 (s, O–H), 2970 (m, C–H), 1682, 1628 (m, C=O), 1602 (m, C=C), 1578 (m, N–H), 1523 (s, N=N), 1369, 1132 (s, C–N), 1283, 1182 (s, C–F), 828, 792, 757 (m, Ph–H). Anal. Calcd for LaC₄₉H₃₉F₉N₇O₇: C, 51.27; H, 3.42; N, 8.54. Found: C, 51.23; H, 3.45; N, 8.52.

Eu(tfd)₂(dmPBPM)(CF₃CO₂) (V). Dark red solid (0.30 g, yield 85%); mp 248–249 °C; ESI(+)-MS (*m/z*, methanol) 1048.1 [M⁺]; ¹H NMR (400 MHz, DMSO-*d*₆) δ ppm = 9.75 (s, 1H), 8.47 (d, *J* = 4.2 Hz, 2H), 7.80–7.74 (m, 10H), 7.25 (s, 9H), 6.82 (d, *J* = 9.0 Hz, 2H), 6.59 (s, 3H), 4.40 (s, 2H), 4.30 (s, 4H), 3.07 (s, 6H). FT-IR (KBr, cm⁻¹): 3423 (s, O–H), 2973 (m, C–H), 1686, 1629 (m, C=O), 1602 (m, C=C), 1576 (m, N–H), 1538 (s, N=N), 1369, 1132 (s, C–N), 1286, 1185 (s, C–F), 825, 792, 762 (m, Ph–H). Anal. Calcd for EuC₄₉H₃₉F₉N₇O₇: C, 50.70; H, 3.39; N, 8.45. Found: C, 50.61; H, 3.33; N, 8.39.

[Gd(tfd)₂(dmPBPM)(CF₃CO₂)] (VI). Red solid (0.26 g, yield 74%); mp 268–269 °C; ESI(+)-MS (*m/z*, methanol) 1053.1 [M⁺]. FT-IR (KBr, cm⁻¹): 3442 (s, O–H), 2917 (m, C–H), 1687, 1629 (m, C=O), 1602 (m, C=C), 1576 (m, N–H), 1539 (s, N=N), 1369, 1133 (s, C–N), 1286, 1185 (s, C–F), 858, 825, 792, 762 (m, Ph–H). Anal. Calcd for GdC₄₉H₃₉F₉N₇O₇: C, 50.46; H, 3.37; N, 8.41. Found: C, 50.33; H, 3.35; N, 8.49.

PMMA Thin Film Preparation. PMMA (100.0 mg) was dissolved in dichloromethane (10.0 mL) with mild sonication for 10 min. The compound (10.0 mg) was added to this solution, which was sonicated mildly for another 15 min. The polymer thin film with similar thickness was coated on a 12 mm × 45 mm quartz plate substrate.

Measurements of Photoisomerization Quantum Yields and Isomerization Rate Constants. UV light (365 nm) was acquired from a ZF-2 UV analyzer (Shanghai Yihui). Visible light (450 nm) was obtained from a 300 W Xe lamp (PLS-SXE300CUV) and isolated using a sharp cutoff filter. A 1 cm path length quartz cell was used for the photoisomerization measurements. The sample concentration was approximately 2.0×10^{-5} M for all complexes. The light intensity was measured by a UV-A radiation meter (Optical electrical apparatus factory of Beijing Normal University). The photoisomerization quantum yield was evaluated based on eq a^{18,30}

$$\Phi = k_0 \frac{1}{I_0} \frac{1}{1 - 10^{-\epsilon c l}} \quad (\text{a})$$

where k_0 is a zero-order rate constant for the decrease of the initial isomer concentration in $\text{mol L}^{-1} \text{s}^{-1}$, I_0 is the intensity of incident irradiation light in $\text{einstein L}^{-1} \text{s}^{-1}$, ϵ is the extinction coefficient in $\text{L mol}^{-1} \text{cm}^{-1}$ at the irradiation wavelength of the solution, c is the concentration of the solution in mol L^{-1} , and l is the path length of light through the sample in cm. The trans-to-cis photoisomerization or cis-to-trans thermal isomerization obeyed first-order kinetics, so the isomerization rate constant, k_{iso} , was calculated from the change in absorbance at a certain wavelength with time by eq b^{19,31}

$$\ln \frac{A_\infty - A_0}{A_\infty - A_t} = k_{\text{iso}} t \quad (\text{b})$$

where A_t , A_0 , and A_∞ denote the absorbance at time t , time zero, and at the end of the reaction, respectively. The data of the quantum yields and the rate constants for all compounds were the average of the three independent replicates performed for each concentration.

The thermal recoverable experiment was performed by a solution of the ligand or the complex in a 1 cm quartz cuvette irradiated with a 365 nm UV lamp for 30 min, and then the cuvette was placed in the thermostated cell of a spectrophotometer, and the spectrum was measured as a function of time or as a function of temperature. The temperature error was controlled as ± 1 °C.

The uncertainty of the quantum yields and the rate constants for all compounds were calculated according to three independent replicates performed for each concentration.

Structure Determination of Complexes I, II, IV, and VI by X-ray Diffraction. Diffraction intensity data for single crystals of the complexes were collected on a Bruker SMART Apex CCD diffractometer equipped with graphite-monochromatic Mo $K\alpha$ ($\lambda = 0.71073$ Å) radiation using the ω scan mode at 173(2) K. The crystal data integration and reduction steps were performed using the SAINT software. Lorentz-polarization and empirical absorption corrections were applied to the data. Structures were solved by direct methods and refined by full-matrix least-squares calculations based on F^2 using the SHELXTL-2014 software package.³² All non-hydrogen atoms were refined anisotropically. Treatment of hydrogen atoms in the least-squares refinement resulted in different data, where some of the hydrogen atoms were constrained by locating them at the calculated positions and the others were independent. Crystallographic details for complexes I, II, IV, and VI are summarized in Table 1. Data for the crystal structures of complexes I, II, IV, and VI have been deposited at the Cambridge Crystallographic Data Centre (CCDC 1437962, 1437960, 1437963, and 1437961 for complexes I, II, IV, and VI, respectively); these data are obtainable free of charge via the Internet at www.ccdc.cam.ac.uk/conts/retrieving.

RESULTS AND DISCUSSION

X-ray Crystallographic Analysis. Suitable crystals of complexes $\text{La}(\text{tfd})_2(\text{PBPM})(\text{CF}_3\text{CO}_2)$ (I), $\text{Eu}(\text{tfd})_2(\text{PBPM})(\text{CF}_3\text{CO}_2)$ (II), $\text{La}(\text{tfd})_2(\text{dmPBPM})(\text{CF}_3\text{CO}_2)$ (IV), and

$\text{Gd}(\text{tfd})_2(\text{dmPBPM})(\text{CF}_3\text{CO}_2)$ (VI) were obtained by slow evaporation from their DMF and ethanol mixed solutions after approximately 1 month. Unit cell determinations and further analyses revealed that all four complexes crystallized in the monoclinic $P2_1/c$ space group with very similar lattice parameters. The molecular geometry of the crystal structures was determined by single-crystal X-ray crystallography. The crystallographic data are provided in Table 1, and selected bond lengths and angles of the coordination environment of the metal centers are listed in Tables S1 and S2 in the Supporting Information. These four complexes were isomorphous, forming a monocapped highly twisted square antiprism. The PBPM (or dmPBPM) ligand chelates with the lanthanide in a tetradentate fashion through one oxygen and three nitrogens from the bis(pyridin-2-ylmethyl)benzohydrazide group. Two pairs of oxygens from the 4,4,4-trifluoro-1-phenylbutane-1,3-dionate (tfd) ligands chelate with the lanthanide ion in a normal way. The coordination sphere is completed by a trifluoroacetate (CF_3COO^-) to give a nine-coordinate lanthanide center with a $\{\text{LnN}_3\text{O}_6\}$ coordination environment, corresponding to a formula of $[\text{Ln}(\text{L})(\text{tfd})_2(\text{CF}_3\text{CO}_2)]$ (L = PBPM or dmPBPM). In the structures of complex I, II, and VI, the distorted monocapped square antiprism has the N(6), O(1), O(6), and O(3) four atoms forming one face, the N(4), O(5), O(2), and N(5) four atoms forming the opposite face, and the atom O(4) occupies the capped position, while in the structure of complex IV, because the trifluoroacetate anion was close to the pyridine group with the N(6) atom, the distorted monocapped square antiprism has the O(6), N(6), O(5), and O(3) four atoms forming one face, the O(1), N(4), N(5), and O(2) four atoms forming the opposite face, and the atom O(4) occupies the capped position. The Ln–O bond lengths are in the range of 2.460–2.508 Å for complex I, 2.331–2.394 Å for complex II, 2.467–2.523 Å for complex IV, and 2.361–2.420 Å for complex VI. The Ln–N bond lengths are in the range of 2.734–2.861 Å for complex I, 2.614–2.748 Å for complex II, 2.732–2.867 Å for complex IV, and 2.633–2.767 Å for complex VI, which are in agreement with the typical values for some lanthanide complexes previously reported.^{22,33} Complexes I and IV have similar ranges of La–O and La–N bond distances, presumably because the individual La–O and La–N bond distances are very similar. The ligands in both La(III) complexes (I and IV) are virtually “identical” except for a long-range *p*-dimethylamino substituent in the dmPBPM ligand; however, the *p*-dimethylamino substituent results in a shortened bond length of the azo group in complex IV. The lengths of N=N bonds in complexes I, II, IV, and VI are 1.201(8), 1.163(8), 1.179(7), and 1.186(13) Å, respectively, which are all slightly shorter than the corresponding distances observed for pure azobenzene and its derivatives.³⁴ Taking complex I as an example, the perspective view of the molecular structure, unit cell packing diagram, and its coordination polyhedron geometry of central La(III) are shown in Figure 1; the others are displayed in Figures S1–S3.

Thermal Analysis of the Complexes. To provide more insight into the structure of the complexes, the thermal stability of complexes I–VI was investigated under a nitrogen atmosphere by thermogravimetric analysis (TGA) in the temperature range of 30–800 °C on the powder samples. As shown in Figure 2, the TG plots provide evidence that complexes I–III exhibit a very similar thermal decomposition process and complexes IV–VI also have the same trend. All complexes underwent no decomposition below 240 °C. The

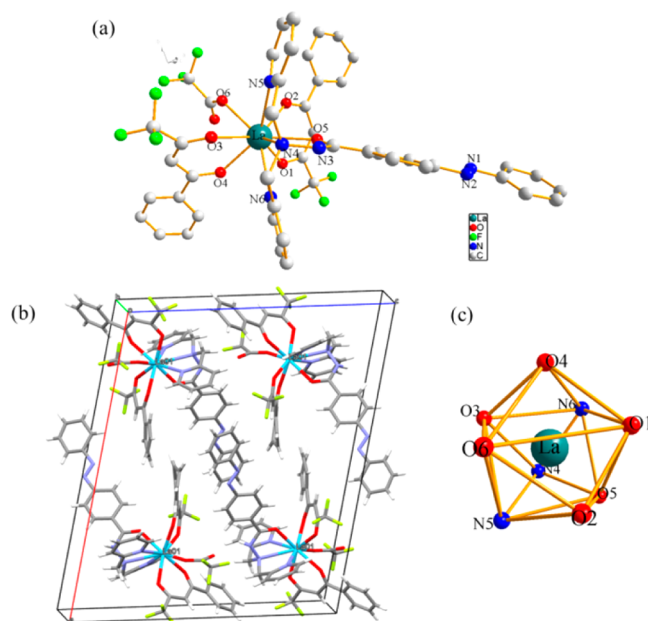


Figure 1. Crystal structure of complex $[\text{La}(\text{tfd})_2(\text{PBPM})(\text{CF}_3\text{CO}_2)]$ (I) (all hydrogen atoms are omitted for clarity) (a), coordination polyhedron geometry of the central La(III) (b), and the packing diagram in the unit cell (c).

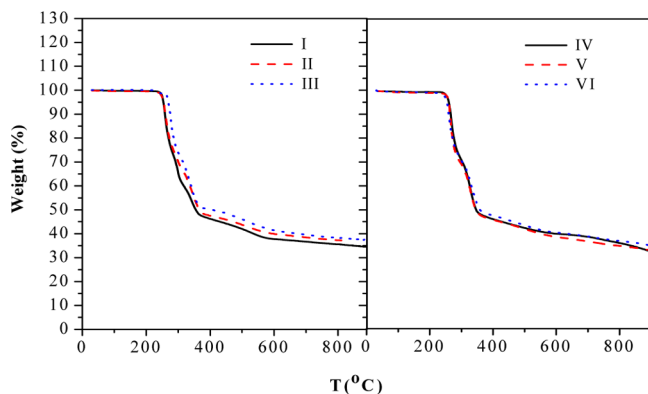


Figure 2. Thermogravimetric analysis (TGA) curves of complexes $[\text{Ln}(\text{tfd})_2(\text{PBPM})(\text{CF}_3\text{CO}_2)]$ (I for La, II for Eu, III for Gd) and $[\text{Ln}(\text{tfd})_2(\text{dmPBPM})(\text{CF}_3\text{CO}_2)]$ (IV for La, V for Eu, VI for Gd).

first decomposition stage occurred in the temperature range of 242–368 °C with a mass loss of 50.35%, 49.21%, and 48.93% for complexes I, II, and III, respectively. The percentages are consistent with material decomposition and elimination of one trifluoroacetate anion and two tfd dianions from the complexes. The theoretically calculated losses are 49.36%, 48.74%, and 48.56% for complexes I, II, and III, respectively. Upon further heating, the complexes started to decompose up to 800 °C. Similarly, the TGA curves showed the first stage mass losses 48.68%, 47.98%, and 47.19% for complexes IV, V, and VI from 244 to 363 °C, respectively, indicating the relative mass loss of one trifluoroacetate anion and two tfd dianions from the complexes. These data are consistent with the theoretically calculated losses of 47.51%, 46.94%, and 46.76% for complexes IV, V, and VI, respectively. From the thermal analysis it could be inferred that the trifluoroacetate anion and tfd dianion are more easily removed from the complexes than the PBPM or dmPBPM ligands, indicating that the designed PBPM and

dmPBPM ligands are strongly coordinating tetradentate ligands.

UV–Vis Absorption Spectra. The UV–vis absorption spectra of free ligands Htfd, PBPM, and dmPBPM and their complexes I–VI in ethanol and acetonitrile at room temperature are displayed in Figure 3, and the spectral data are listed

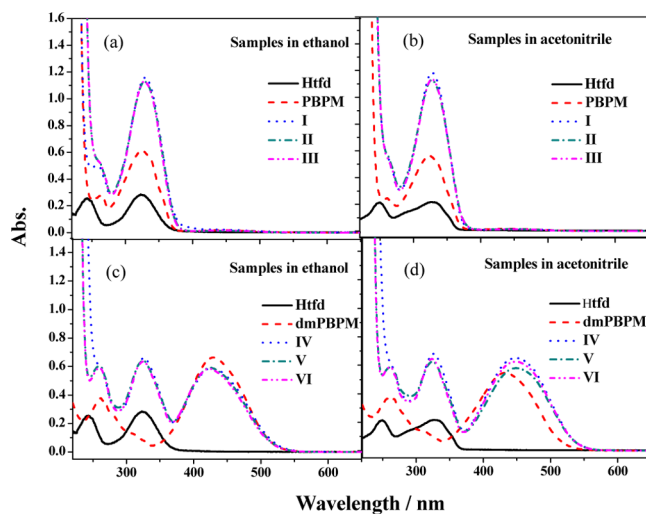


Figure 3. UV–vis absorption spectra of PBPM, complexes $[\text{Ln}(\text{tfd})_2(\text{PBPM})(\text{CF}_3\text{CO}_2)]$ (I for La, II for Eu, III for Gd) (a, b) and dmPBPM, complexes $[\text{Ln}(\text{tfd})_2(\text{dmPBPM})(\text{CF}_3\text{CO}_2)]$ (IV for La, V for Eu, VI for Gd) (c, d) (2.0×10^{-5} mol/L) in different solvents.

in Table S3. As shown in Figure 3, the UV–vis absorption spectrum of the ligand PBPM exhibits two typical absorption bands of the azo group in the region of 250–500 nm, a strong $\pi-\pi^*$ transition band (325 nm/ 3.07×10^4 L mol $^{-1}$ cm $^{-1}$), and a weak absorption band (440 nm/ 900 L mol $^{-1}$ cm $^{-1}$) from the forbidden symmetry of the $n-\pi^*$ transition. However, owing to the contribution of the electronic-donating substituent, the *N,N*-dimethylamino group, dmPBPM exhibits only strong intensity $\pi-\pi^*$ (268 nm/ 1.80×10^4 , 428 nm/ 3.31×10^4 L mol $^{-1}$ cm $^{-1}$) absorption bands. The broad band around 350–550 nm of dmPBPM may be attributed to the red shift of the $\pi-\pi^*$ band arising from the strong electron-donating group, leading to the weak $n-\pi^*$ transition absorption band buried in its $\pi-\pi^*$ band.^{1,22}

The spectra of complexes I–VI show the iteration of the free ligands tfd and PBPM (or dmPBPM) absorption spectra, accompanied by a small red shift at the maximum wavelength. Likewise, the spectra of complexes I–VI show a strong azo group $\pi-\pi^*$ transition absorption close to 328 nm and the symmetry forbidden $n-\pi^*$ transition within the range of 400–500 nm. Furthermore, the molar absorption coefficients of complexes I–VI around 328 nm are almost doubled compared with those of the free ligands PBPM or dmPBPM (shown in Table S3), perhaps owing to the simple iteration of the two localized chromophores from the free ligands tfd and PBPM (or dmPBPM), and also the ligands absorption being perturbed by lanthanide ion coordination. Finally, no significant effect of the solvent polarity on the absorption spectra of complexes I–VI was observed.

Photoisomerization Behavior of PBPM and dmPBPM Ligands. Figure 4 shows the absorption spectral changes of PBPM and dmPBPM upon UV irradiation at 365 nm and visible-light irradiation at 450 nm as a function of time in an

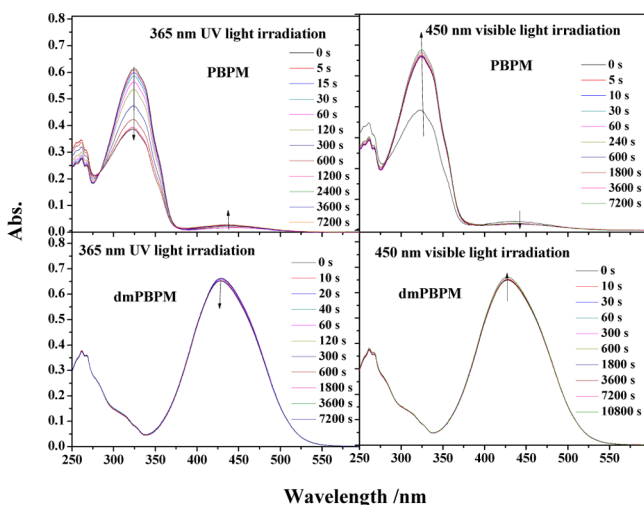


Figure 4. UV-vis spectral changes of PBPM and dmPBPM in ethanol solution (2.0×10^{-5} mol/L) upon irradiation at 365 nm and recoverable irradiation at 450 nm as a function of time.

ethanol solution. The similar absorption spectral changes in acetonitrile solution are shown in the Supporting Information (Figure S4). For PBPM, the intensity of the $\pi-\pi^*$ absorption band at 325 nm gradually decreased with increasing irradiation time, while the absorbance at 440 nm ($n-\pi^*$ transitions band) increased. A photostationary state was reached after 10 min, which indicates completion of isomerization from trans to cis. Subsequently, irradiation of the solution with visible light (450 nm) led to 80% recovery of the absorption spectrum. This reversible spectral change was observed repeatedly (Figure S5). Ten cycles of maximum absorption intensity at 325 and 440 nm were modulated by the irradiation of UV light at 365 nm and visible light at 450 nm, alternatively, which exhibited no variation. The first-order rate constants of the photoisomerization reaction of PBPM in solutions were $3.0 \times 10^{-3} \text{ s}^{-1}$ in ethanol and $2.0 \times 10^{-3} \text{ s}^{-1}$ in acetonitrile, which are much higher than those of azobenzene and its derivatives (10^{-5} – 10^{-4} s^{-1}).^{18,19} An estimate of the photoreaction quantum yields ($\Phi_{t \rightarrow c}$) in different solvents was evaluated based on eq a (see Experimental Section). The photoisomerization quantum yields ($\Phi_{t \rightarrow c}$) of PBPM were 0.045 in ethanol and 0.037 in acetonitrile, which are smaller than those of a substituted azobenzene, such as 4-methoxy-4'-nitroazobenzene or 2,4,6-trimethylazobenzene.^{35,36} Data are listed in Table 2. Evidently the spectra of dmPBPM in an ethanol solution underwent no significant change upon irradiation with UV or visible light with increasing time. However, in an acetonitrile solution, the spectra of dmPBPM showed some change under the same conditions (Figure S4). The dielectric constants of ethanol and

acetonitrile are 24.5 and 37.5, respectively. Therefore, acetonitrile can stabilize the cis form to some extent. It should be mentioned that even though observed in acetonitrile, the photoisomerization of dmPBPM was still much less than that of PBPM. The electron-donating group reduces the $\pi-\pi^*$ energy level of the azo group; therefore, the energy difference between the $\pi-\pi^*$ level and the $n-\pi^*$ level decreased, resulting in the fact that the spectrum showed different changes in different solvents as far as the absorption intensity was concerned. It appears that the para electron-donating substituent *N,N*-dimethylamino group produced substantial changes on the absorption and was unfavorable to the photoisomerization properties of azobenzene in the molecules.

Photoisomerization Behavior of Complexes I–VI.

Complexes I–III ($[\text{Ln}(\text{tfd})_2(\text{PBPM})(\text{CF}_3\text{CO}_2)]$) constructed from a PBPM ligand showed similar spectral changes upon irradiation in different solvents. Taking complex II ($[\text{Eu}(\text{tfd})_2(\text{PBPM})(\text{CF}_3\text{CO}_2)]$) as an example, Figure 5 shows the

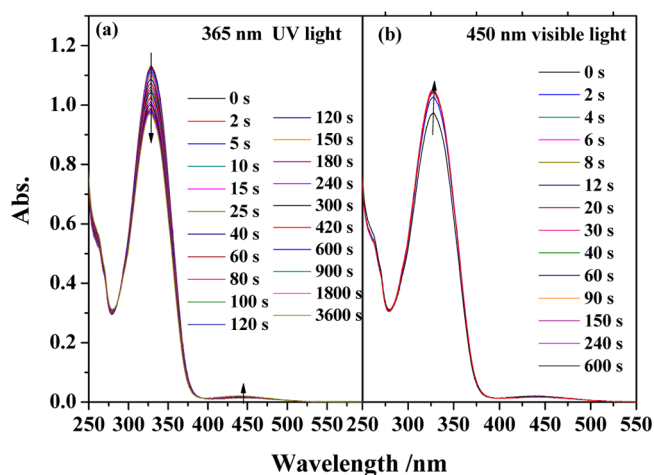


Figure 5. UV-vis spectral change of complex II ($[\text{Eu}(\text{tfd})_2(\text{PBPM})(\text{CF}_3\text{CO}_2)]$) in ethanol solution (2.0×10^{-5} mol/L) upon irradiation at 365 nm and recoverable irradiation at 450 nm as a function of time.

typical spectral change of complex II in an ethanol solution upon irradiation with 365 nm and its recoverable spectra after irradiation with 450 nm. The absorption maximum of complex II in ethanol solution appeared at 328 nm, characteristic of the $\pi-\pi^*$ absorption band, with a very weak $n-\pi^*$ absorption band at 448 nm. Upon UV 365 nm light irradiation, a band at 448 nm was developed at the expense of the corresponding original band at 328 nm with two isosbestic points located at 287 and 386 nm. This spectral change indicates the occurrence of the photoisomerization in solution. The complex reached a photostationary state within 10 min with irradiation at 365 nm.

Table 2. Quantum Yields ($\Phi_{t \rightarrow c}$) and Photoisomerization Rate Constants (s^{-1}) of PBPM, dmPBPM, and Complexes I–VI in Different Solvents

compounds	ethanol		acetonitrile		compounds	ethanol		acetonitrile	
	$10^2\Phi_{t \rightarrow c}$	10^4k_{iso}	$10^2\Phi_{t \rightarrow c}$	10^4k_{iso}		$10^4\Phi_{t \rightarrow c}$	10^4k_{iso}	$10^4\Phi_{t \rightarrow c}$	10^4k_{iso}
PBPM	4.5 ± 0.4	30.0 ± 1.5	3.7 ± 0.3	20.1 ± 1.1	dmPBPM	<i>a</i>	<i>a</i>	0.74 ± 0.1	<i>a</i>
I	3.9 ± 0.4	40.1 ± 1.9	1.1 ± 0.1	13.0 ± 0.6	IV	<i>a</i>	<i>a</i>	<i>a</i>	<i>a</i>
II	3.6 ± 0.3	50.0 ± 2.1	2.5 ± 0.2	26.3 ± 1.2	V	0.67 ± 0.1	0.49 ± 0.02	1.90 ± 0.4	0.99 ± 0.4
III	3.8 ± 0.3	30.2 ± 1.3	2.8 ± 0.2	20.5 ± 1.2	VI	1.80 ± 0.3	1.11 ± 0.05	0.83 ± 0.2	<i>a</i>

^aNo significant photoisomerization behavior was observed.

When the UV irradiation was ceased, 75% of the compound returned to the trans form with visible 450 nm irradiation for 2 s. The recovery percentage of the trans form was a little lower than that of the pure PBPM ligand, because the photochemical pathway was not simple in such a complex, where the visible absorption would be a mixture of other bands, not just the azo $n-\pi^*$ band. Similar spectral changes for complex **II** in an acetonitrile solution are shown in Figure S6.

The photoisomerization reaction of complex **II** in solutions followed first-order kinetics with rate constants of $5.0 \times 10^{-3} \text{ s}^{-1}$ in ethanol and $2.6 \times 10^{-3} \text{ s}^{-1}$ in acetonitrile and quantum yields of 0.039 in ethanol and 0.011 in acetonitrile (Table 2), which are similar to that of pure PBPM. Compared with other azobenzene-containing metal complexes, such as lanthanide-coordinated complexes show active photoisomerization. The trans-to-cis photoisomerization quantum yields are comparable with their pure ligands. It is obvious that the trans-to-cis photoisomerization rates of complexes **I–III** (10^{-2} s^{-1}) are comparable to or even higher than those of the reported Ru(II) or Rh(III) bis(terpyridine) metal complexes (10^{-5} – 10^{-3} s^{-1}),¹⁹ as well as azobenzene itself (10^{-5} – 10^{-4} s^{-1}).^{18,36}

To test the stability of the trans–cis–trans photoisomerization, 10 cycles of complex **II** switching in different solvent were conducted by irradiating the sample with 365 nm light for 10 min, followed by 450 nm light for 2 min. Complex **II** was stable under these conditions (Figures 6 and S7), and no signs of

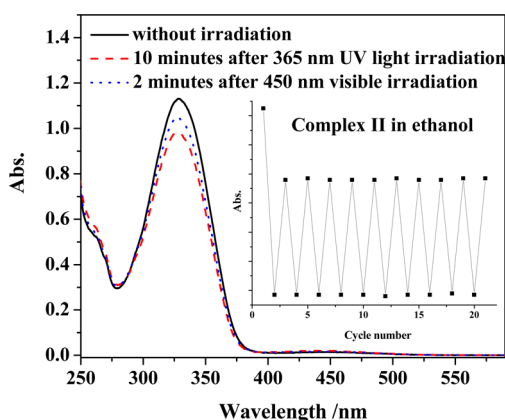


Figure 6. UV–vis spectral changes of complex **II** ($[\text{Eu}(\text{tfd})_2(\text{PBPM})(\text{CF}_3\text{CO}_2)]$) in ethanol solution ($2.0 \times 10^{-5} \text{ mol/L}$) by irradiation of UV light at 365 nm and visible light at 450 nm. (Inset) Ten cycles of the maximum absorption intensity at 328 and 448 nm alternatively modulated by irradiation of UV light at 365 nm and visible light at 450 nm.

photodegradation were detected. The UV–vis absorption spectra changes of complexes **I** and **III** in ethanol and acetonitrile solutions were similar to those of complex **II** (Figures S8–S10 in the Supporting Information). Complexes **I–III** showed an overall reversible isomerization reaction, and more than 10 cycles could be repeated, demonstrating their excellent fatigue resistance and reversibility. The good reversibility of trans–cis–trans photoisomerization of these complexes in solutions denied the possibility of photodegradation.

Different from complex **I** ($[\text{La}(\text{tfd})_2(\text{PBPM})(\text{CF}_3\text{CO}_2)]$), complex **IV** ($[\text{La}(\text{tfd})_2(\text{dmPBPM})(\text{CF}_3\text{CO}_2)]$) was unstable under UV light irradiation both in ethanol and in acetonitrile solutions, simply owing to the dmPBPM ligand that bears the

electron-donating dimethylamino group. Although the absorption maximum at 426 nm could decrease upon UV 365 nm irradiation and be recovered by 450 nm irradiation (Figure S11), the absorption intensity at 326 nm, which can be assigned to the main absorption of the tfd ligand, decreased upon irradiation with UV 365 nm light or visible 450 nm light. This spectral change indicated the occurrence of the photobleaching of complex **IV** in solution, where the tfd ligand was removed from the molecule. There are two reasons to interpret the instability of complex **IV** in the solution state under UV irradiation. First, La(III) is the most kinetically labile among the lanthanide ions.³⁷ Its complexes are not as stable as the complexes of other lanthanide ions. Second, the dmPBPM is larger in size than PBPM due to the electron-donating dimethylamino group.

Compared with the easy-to-observe photoisomerization properties of PBPM, the quantum yield and photoisomerization rate constants of dmPBPM were too low to be determined. It was interesting that complexes **V** and **VI** containing dmPBPM showed a more sensitive photoisomerization than dmPBPM itself. This indicates that the mechanism of the isomerization is mediated through the ligand excited states. The coordination of a lanthanide ion presumably increased the spin–orbit coupling which allowed isomerization to occur. As shown in Figures S12 and S13, upon UV 365 nm light irradiation in different solvents, complexes **V** and **VI** exhibited a similar trend to that of dmPBPM. With the photoisomerization, the intensities of the bands at 325 and 426 nm decreased, accompanied by a small red shift of the band around 426 nm. When irradiating the sample using 450 nm light, the absorption intensities around 325 and 426 nm increased. The quantum yields of isomerization of complexes **V** and **VI** are much smaller than those of PBPM and complexes **I–III** owing to the para electron-donating substituent, the dimethylamino group in dmPBPM ligand (Table 2).

Photoisomerization Behavior of PBPM and Complexes **I–III in PMMA Film.** PBPM and its complexes **I–III** presented good reversible and repeatable photoisomerization reactions in solutions. For the purpose of implementing such photoresponsive substances to practical applications, their reversible photoisomerization in the solid state was also studied. The measurements of the UV–vis absorption spectra of PBPM and complexes **I–III** doped in PMMA film were performed. The PBPM isomerization behavior in PMMA film showed a similar trend to that in solution (Figure S14). Upon irradiation with 365 nm UV light, the intensity of its $\pi-\pi^*$ transition absorption band at 328 nm decreased while its $n-\pi^*$ transition absorption band at 440 nm gradually increased. A photostationary state was reached after 10 min. Subsequently, irradiating the solution with visible light at 450 nm for only 5 s led to 80% recovery of the absorption spectra, indicating that its cis form was unstable in PMMA film. The cis form could easily and quickly transfer to its trans form. This reversible spectral changes were also observed repeatedly (Figure S16a). The first-order rate constant of the photoisomerization reaction of PBPM in PMMA was $3.1 \times 10^{-4} \text{ s}^{-1}$, very close to that obtained in solution.

The UV–vis spectral changes of complex **I** in a PMMA film upon irradiation at 365 nm and its recoverable spectra upon irradiation at 450 nm are shown in Figure S15. The $\pi-\pi^*$ absorption band of complex **I** in a PMMA film also appeared at 329 nm, and a weak $n-\pi^*$ absorption band was observed at 450 nm, with two isosbestic points located at 287 and 386 nm,

respectively. Upon 365 nm UV light irradiation, the maximum absorption intensity at 450 nm increased accompanied by a decrease of the intensity at 329 nm. A photostationary state was reached in just 10 min with irradiation at 365 nm. The first-order reaction rate constant of trans to cis for complex I in PMMA film was $7.4 \times 10^{-3} \text{ s}^{-1}$, which is higher than those in solution and for PBPM itself. When the UV irradiation was ceased, 75% of the system returned to the trans form with 450 nm irradiation for 30 s. The recovery of the trans form by visible light demonstrates that the photochemical pathway of complex I is similar to those in solution and for PBPM itself.

Moreover, complex I was stable in PMMA without signs of photodegradation when undergoing 10 cycles of alternating irradiation of UV light at 365 nm and visible light at 450 nm (Figure S16b). Complex III showed similar isomerization properties as those of complex I (Figure S17). The first-order reaction rate constant for trans-to-cis isomerization of complex III in PMMA film was $5.0 \times 10^{-3} \text{ s}^{-1}$, which was also higher than those in solution and for PBPM itself. In the same condition, complex II showed a poor photoisomerization reaction owing to its insolubility in PMMA.

Thermal Cis-to-Trans Isomerization of PBPM and Complexes I–III. PBPM and its complexes I–III were sensitive to light-triggered azobenzene trans-to-cis isomerization with 365 nm light. The isomerization could be reversed by irradiation with visible light at 450 nm, which also occurred spontaneously in the dark, because of the thermodynamic stability of the trans isomer.¹ Cis-to-trans thermal isomerization can range from an order of hours to days for azobenzenes and from seconds to milliseconds for pseudostilbenes.^{38,39} To examine the cis-to-trans thermal isomerization of the ligands and complexes, first, the solutions of PBPM and complexes I–III in ethanol or acetonitrile were irradiated for 30 min at 365 nm light and then kept in the dark at room temperature; they began to reverse to the trans isomer after standing in the dark for 16 h and longer, which was too slow to find the first-order rate constants and half-life. The reverse process of cis-to-trans isomerization was actively monitored by UV–vis absorption spectroscopy at 50 °C. The calculated first-order rate constants (k) and half-life time ($\tau_{1/2}$) for this process are presented in Table 3. A representative example is shown in Figure 7, and the

Table 3. Thermal Isomerization Rate Constants (k_{iso} , s^{-1}) and Half-Life ($\tau_{1/2}$, min) of PBPM and Complexes I–III in Different Solvents at 50 °C

compounds	ethanol		acetonitrile	
	$10^4 k_{\text{iso}}$	$\tau_{1/2}$	$10^4 k_{\text{iso}}$	$\tau_{1/2}$
PBPM	2.2 ± 0.11	52.5 ± 2.6	0.65 ± 0.03	105.6 ± 4.8
I	2.4 ± 0.12	47.8 ± 2.3	1.9 ± 0.08	62.4 ± 2.5
II	3.0 ± 0.15	37.8 ± 1.9	2.7 ± 0.14	41.9 ± 2.1
III	1.8 ± 0.08	64.5 ± 3.4	1.6 ± 0.07	72.9 ± 3.1

others are organized in Figure S18. At 50 °C, the first-order rate constants for the cis-to-trans thermal isomerization of PBPM and complexes I–III in ethanol and acetonitrile solutions are larger than those of other azobenzene-containing metal complexes and smaller than those of organic pull–push azobenzene.^{24,40,41}

The behavior of the thermal cis-to-trans isomerization of both ligand PBPM and complexes I–III as a function of temperature was also examined in ethanol (Figure S19). In contrast to the PBPM, it was found that the rate of the thermal

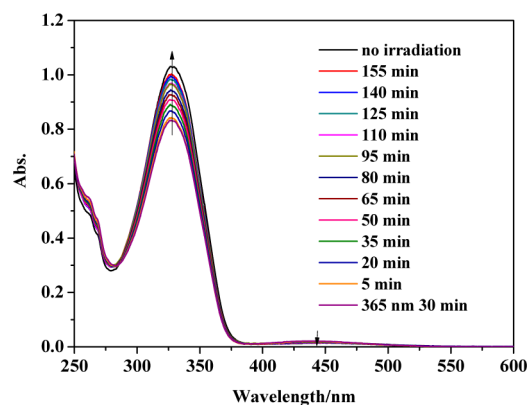


Figure 7. UV–vis spectral changes before and after 30 min irradiation with 365 nm, and thermal cis-to-trans isomerization of complex I ($[\text{La}(\text{tfd})_2(\text{PBPM})(\text{CF}_3\text{CO}_2)]$) in ethanol solution ($2.0 \times 10^{-5} \text{ mol/L}$) at 50 °C.

isomerization of the Ln(III) complex was higher. For instance, at 70 °C for 15 min, PBPM was able to achieve 70% cis-to-trans reversal while the La(III), Gd(III), and Eu(III) complexes accomplished 85%, 95%, and 100% reversal, respectively. At 78 °C for 15 min, the refluxing temperature of ethanol, all ligands and complexes can achieve 100% recovery. In the solid state, the PMMA film of PBPM ligand and its Ln(III) complexes were able to recover 100% at 80 °C.

As far as dmPBPM and complexes IV–VI are concerned, since the cis form was difficult to be obtained under the same conditions, the thermal stability of the cis forms of dmPBPM and complexes IV–VI was not investigated.

Photoluminescent Properties of Complexes II and V.

It is well established that some Eu(III) complexes involving β -diketonates would yield bright red emission under near-ultraviolet or visible-light irradiation owing to the efficient energy transfer from the β -diketonate ligand to the central Eu(III) ions (antenna effect).^{42–44} Their unique optical properties, such as narrow emission bands, high luminescence efficiency, and long excited-state lifetimes, have resulted in them being of interest for a wide range of photonic applications including light-emitting diodes, a laser system, and luminescent probes for bioanalyses.^{27,33,45–52} We therefore investigated the luminescent properties of europium complexes II and V in ethanol and acetonitrile solutions at room temperature. The photoluminescence spectra of complexes II and V in different solvents are shown in Figure 8. Upon excitation at 330 nm, complexes II and V showed the characteristic emission bands of an Eu(III) ion originating from the $^5\text{D}_0 \rightarrow ^7\text{F}_j$ ($J = 0–4$) transitions. Among them, the induced electric dipole transition of $^5\text{D}_0 \rightarrow ^7\text{F}_2$ at 614 nm was the strongest. The intensity of emission bands at 578, 590, and 650 nm corresponding to the $^5\text{D}_0 \rightarrow ^7\text{F}_{0,1,3}$ transitions were relatively weak owing to the magnetic and electric dipole-forbidden schemes. The overall luminescence quantum yields (Φ_0) were determined experimentally under excitation of the ligand in acetonitrile and ethanol solutions at room temperature. The Φ_0 values of complexes II and V in ethanol were 0.049 and 0.028, respectively, which were slightly lower than those obtained in acetonitrile solvent (0.074 for II and 0.034 for V). By comparing the absorption spectra of complexes II and V with their excitation spectra, it was observed that the excitation and absorbance spectra of complexes II and V overlapped well with the tfd dionate ligand, indicating that Eu(III) emission was

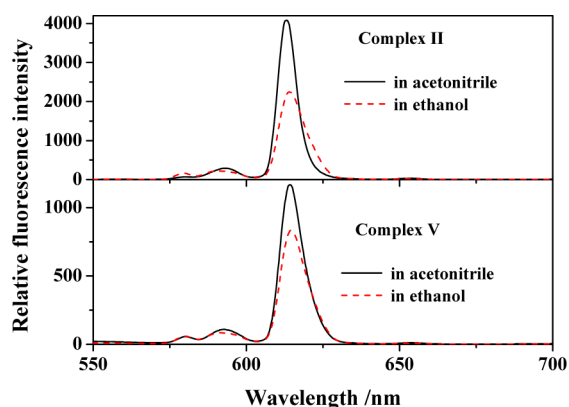


Figure 8. Emission spectra of complexes **II** ($[\text{Eu}(\text{tfd})_2(\text{PBPM})(\text{CF}_3\text{CO}_2)]$) ($\lambda_{\text{ex}} = 355$ nm) and **V** ($[\text{Eu}(\text{tfd})_2(\text{dmPBPM})(\text{CF}_3\text{CO}_2)]$) ($\lambda_{\text{ex}} = 370$ nm) in different solvents (2.0×10^{-5} mol/L).

mainly sensitized from the tfd dionate ligand. The ancillary ligands of PBPM and dmPBPM did not participate in the energy transfer to the lanthanide ion, which might be attributed to their lower triplet state energy levels. To gain insight into the nature of the electronic transitions of the systems, TD-DFT was carried out for geometry optimization and the excitation energies of the lowest excited triplet states of tfd, PBPM, and dmPBPM were calculated to be 2.4817, 1.7846, and 1.8328 eV, respectively. Obviously, the excitation energies of the lowest excited triplet states of both PBPM and dmPBPM are lower than the resonance level of the Eu^{3+} ion ($^5\text{D}_0$, 2.1434 eV), which agrees well with the experimental results. Hence, the experimental results prove the theoretical prediction, where only the excitation energy of tfd could be transferred to the rare earth ion according to the triplet state of the ligand being higher than the resonance level of the rare earth ion.⁵³ Furthermore, the luminescence intensity did not change upon UV–vis light irradiation (Figure S20). As a result, the present findings demonstrate that complex **II** will be a good dual-function smart material for biological system applications and light conversion molecular devices.

Magnetic Properties Studies of Complexes **III** and **VI**.

Since the Gd(III) ion has seven unpaired f electrons with a high magnetic moment and long electronic relaxation time, it has been intensively investigated for magnetic refrigeration and magnetic resonance imaging materials.^{54–59} The magnetic properties of the synthesized $[\text{Gd}(\text{tfd})_2(\text{PBPM})(\text{CF}_3\text{CO}_2)]$ (**III**) and $[\text{Gd}(\text{tfd})_2(\text{dmPBPM})(\text{CF}_3\text{CO}_2)]$ (**VI**) complexes have also been studied. The variable-temperature molar magnetic susceptibilities χ_M of complexes **III** and **VI** were measured under an applied field of 1000 Oe and in the range of 2–300 K. The $\chi_M T$ versus T plots are shown in Figure 9. The room-temperature $\chi_M T$ values of complexes **III** and **VI** were found to be 8.85 and 9.65 $\text{cm}^3 \text{K mol}^{-1}$, respectively, which are a little higher than the theoretical values (7.94) owing to the orbital magnetic moment contribution to the central ion.⁶⁰ Since the shortest distance of the nearest Gd(III) ions between the adjacent molecules was 9.695 Å, it can be assumed that no direct magnetic interaction existed with a high possibility of a weak dipole–dipole role among Gd(III) complex molecules.⁶¹ The $\chi_M T$ values for the two complexes hold above 100 K and then slowly decreased down to 12 K because of the single-ion crystal field effects.⁶² The $\chi_M T$ values decreased quickly in the range of 12 K–2 K owing to the zero-field splitting of Gd(III) ions. The $\chi_M T$ data were fitted (χ_M^{-1} versus T) using the

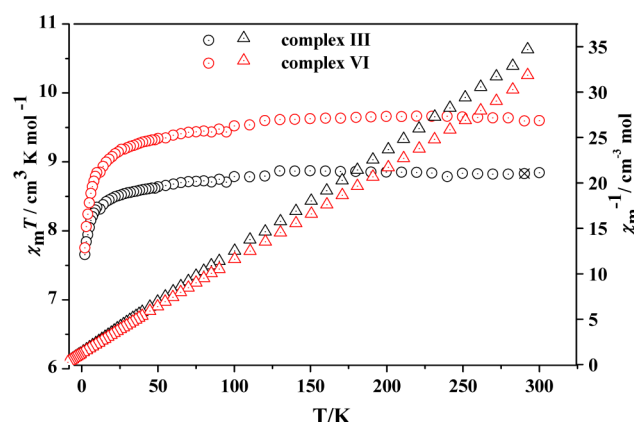


Figure 9. $\chi_M T$ (O) and $1/\chi_M$ (Δ) versus T plots for complexes **III** ($[\text{Gd}(\text{tfd})_2(\text{PBPM})(\text{CF}_3\text{CO}_2)]$) and **VI** ($[\text{Gd}(\text{tfd})_2(\text{dmPBPM})(\text{CF}_3\text{CO}_2)]$) measured at 1000 Oe.

Curie–Weiss equation, and the values of C ($\text{cm}^3 \text{K mol}^{-1}$) and θ (K), obtained from the best fitting, were, respectively, 8.84 and -0.76 for complex **III** and 9.66 and -1.24 for complex **VI**, indicating that both complexes were antiferromagnetic.⁶³

SUMMARY

A series of novel multinary β -diketonate lanthanide complexes (La(III), Eu(III), Gd(III)) of PBPM and dmPBPM functionalized with azobenzene were synthesized and structurally characterized by FT-IR, ^1H NMR, TGA, ESI-MS, and single-crystal X-ray diffraction crystallography. The X-ray crystal structures indicated that the Ln(III) ion was nine coordinate by one oxygen atom and three nitrogen atoms from the PBPM ligand (or dmPBPM), four oxygen atoms from the two β -diketonate ligands, and the one oxygen atom from trifluoroacetate, forming a monocapped twisted square antiprism. The thorough trans-to-cis photoisomerization study of the complexes revealed that all complexes were able to undergo reversible trans-to-cis photoisomerization in different organic solvents as well as in solid PMMA film. The $[\text{Ln}(\text{tfd})_2(\text{PBPM})(\text{CF}_3\text{CO}_2)]$ complexes bearing azobenzene groups without a donor substituent showed a more rapid reversible trans-to-cis photoisomerization compared with that of the $[\text{Ln}(\text{tfd})_2(\text{dmPBPM})(\text{CF}_3\text{CO}_2)]$ complexes. Remarkably, a luminescence investigation demonstrated that the ligands exhibited a good antennae effect with respect to the Eu(III) ion owing to the efficient intersystem crossing and ligand-to-metal energy transfer mechanism, which was confirmed by the TD-DFT calculation. Interestingly, the magnetic properties of the Gd(III) complexes were antiferromagnetic. The present results signified the photoisomerization and photoluminescence dual functions of Eu(III) multinary complexes, which would be anticipated for potential applications as smart materials for biological systems or as a light conversion molecular device.

ASSOCIATED CONTENT

Supporting Information

The Supporting Information is available free of charge on the ACS Publications website at DOI: 10.1021/acs.inorgchem.6b02819.

NMR spectra for ligands and complexes and IR spectra for all complexes (PDF)

X-ray crystallographic files for complexes **I**, **II**, **IV**, and **VI** (CIF)

AUTHOR INFORMATION

Corresponding Authors

*E-mail: linlr@xmu.edu.cn.

*E-mail: mal@uhcl.edu.

ORCID 

Li-Rong Lin: 0000-0002-2521-3809

Author Contributions

[‡]H.-H.T. and Y.-G.W. contributed equally to this work.

Notes

The authors declare no competing financial interest.

ACKNOWLEDGMENTS

This work is supported by the National Natural Science Foundation of China (Grant No. 21271150) and the Natural Science Foundation of Fujian province (Grant No. 2015J01060).

REFERENCES

- (1) Bandara, H. M.; Burdette, S. C. Photoisomerization in Different Classes of Azobenzene. *Chem. Soc. Rev.* **2012**, *41*, 1809–1825.
- (2) Russew, M. M.; Hecht, S. Photoswitches: from Molecules to Materials. *Adv. Mater.* **2010**, *22*, 3348–3360.
- (3) Dong, M.; Babalhavaeji, A.; Samanta, S.; Beharry, A. A.; Woolley, G. A. Red-Shifting Azobenzene Photoswitches for in Vivo Use. *Acc. Chem. Res.* **2015**, *48*, 2662–2670.
- (4) Samanta, S.; Beharry, A. A.; Sadowski, O.; McCormick, T. M.; Babalhavaeji, A.; Tropepe, V.; Woolley, G. A. Photoswitching Azo Compounds in Vivo with Red Light. *J. Am. Chem. Soc.* **2013**, *135*, 9777–9784.
- (5) Dugave, C.; Demange, L. Cis-Trans Isomerization of Organic Molecules and Biomolecules: Implications and Applications. *Chem. Rev.* **2003**, *103*, 2475–2532.
- (6) Yao, C.; Wang, P.; Li, X.; Hu, X.; Hou, J.; Wang, L.; Zhang, F. Near-Infrared-Triggered Azobenzene-Liposome/Upconversion Nanoparticle Hybrid Vesicles for Remotely Controlled Drug Delivery to Overcome Cancer Multidrug Resistance. *Adv. Mater.* **2016**, *28*, 9341–9348.
- (7) Williams, G. V.; Do, M. T.; Middleton, A.; Raymond, S. G.; Bhuiyan, M. D.; Kay, A. J. Optical Modulation of the Diffraction Efficiency in an Indoline Azobenzene/Amorphous Polycarbonate Film. *Nanoscale Res. Lett.* **2016**, *11*, 331–336.
- (8) Sun, H.; Zhao, L.; Wang, T.; An, G.; Fu, S.; Li, X.; Deng, X.; Liu, J. Photocontrolled Reversible Morphology Conversion of Protein Nanowires Mediated by an Azobenzene-Cored Dendrimer. *Chem. Commun.* **2016**, *52*, 6001–6004.
- (9) Deiana, M.; Pokladek, Z.; Olesiak-Banska, J.; Mlynarz, P.; Samoc, M.; Matczyszyn, K. Photochromic Switching of the DNA Helicity Induced by Azobenzene Derivatives. *Sci. Rep.* **2016**, *6*, 28605–28613.
- (10) Zhang, R.; Ji, Y. J.; Yang, L.; Zhang, Y.; Kuang, G. C. A Ferrocene-Azobenzene Derivative Showing Unprecedented Phase Transition and Better Solubility upon UV Irradiation. *Phys. Chem. Chem. Phys.* **2016**, *18*, 9914–9917.
- (11) Perez-Miqueo, J.; Altube, A.; Garcia-Lecina, E.; Tron, A.; McClenaghan, N. D.; Freixa, Z. Photoswitchable Azobenzene-appended Iridium(III) Complexes. *Dalton Trans.* **2016**, *45*, 13726–13741.
- (12) Guerchais, V.; Le Bozec, H. Metal Complexes Featuring Photochromic Ligands. *Top. Organomet. Chem.* **2010**, *28*, 171–225.
- (13) Yan, J. F.; Lin, D. Q.; Wang, X. G.; Wu, K. Q.; Xie, L. L.; Yuan, Y. F. Ferrocenylethynyl-Terminated Azobenzenes: Synthesis, Electrochemical, and Photoisomerization studies. *Chem. - Asian J.* **2015**, *10*, 614–621.
- (14) Kume, S.; Kurihara, M.; Nishihara, H. Reversible Trans-Cis Photoisomerization of Azobenzene-Attached Bipyridine Ligands Coordinated to Cobalt Using a Single UV Light Source and the Co(III)/Co(II) Redox Change. *Chem. Commun.* **2001**, 1656–1657.
- (15) Yamamura, M.; Yamakawa, K.; Okazaki, Y.; Nabeshima, T. Coordination-driven Macrocyclization for Locking of Photo- and Thermal Cis-Trans Isomerization of Azobenzene. *Chem. - Eur. J.* **2014**, *20*, 16258–16265.
- (16) Guezguez, I.; Ayadi, A.; Ordon, K.; Iliopoulos, K.; Branzea, D. G.; Migalska-Zalas, A.; Makowska-Janusik, M.; El-Ghayoury, A.; Sahraoui, B. Zinc Induced a Dramatic Enhancement of the Nonlinear Optical Properties of an Azo-Based Iminopyridine Ligand. *J. Phys. Chem. C* **2014**, *118*, 7545–7553.
- (17) Perez-Miqueo, J.; Telleria, A.; Munoz-Olasagasti, M.; Altube, A.; Garcia-Lecina, E.; de Cozar, A.; Freixa, Z. Azobenzene-Functionalized Iridium(III) Triscyclometalated Complexes. *Dalton Trans.* **2015**, *44*, 2075–2091.
- (18) Sierocki, P.; Maas, H.; Dragut, P.; Richardt, G.; Vogtle, F.; De Cola, L.; Brouwer, F. A.; Zink, J. I. Photoisomerization of Azobenzene Derivatives in Nanostructured Silica. *J. Phys. Chem. B* **2006**, *110*, 24390–24398.
- (19) Yutaka, T.; Mori, I.; Kurihara, M.; Mizutani, J.; Kubo, K.; Furusho, S.; Matsumura, K.; Tamai, N.; Nishihara, H. Synthesis, Characterization, and Photochemical Properties of Azobenzene-Conjugated Ru(II) and Rh(III) Bis(terpyridine) Complexes. *Inorg. Chem.* **2001**, *40*, 4986–4995.
- (20) Yutaka, T.; Mori, I.; Kurihara, M.; Mizutani, J.; Tamai, N.; Kawai, T.; Irie, M.; Nishihara, H. Photoluminescence Switching of Azobenzene-conjugated Pt(II) Terpyridine Complexes by Trans-Cis Photoisomerization. *Inorg. Chem.* **2002**, *41*, 7143–7150.
- (21) Telleria, A.; Pérez-Miqueo, J.; Altube, A.; García-Lecina, E.; de Cozar, A.; Freixa, Z. Azobenzene-Appended Bis-Cyclometalated Iridium(III) Bipyridyl Complexes. *Organometallics* **2015**, *34*, 5513–5529.
- (22) Lin, L. R.; Wang, X.; Wei, G. N.; Tang, H. H.; Zhang, H.; Ma, L. H. Azobenzene-Derived Tris-Beta-Diketonate Lanthanide Complexes: Reversible Trans-to-cis Photoisomerization in Solution and Solid state. *Dalton Trans.* **2016**, *45*, 14954–14964.
- (23) Lima, P. P.; Nolasco, M. M.; Paz, F. A. A.; Ferreira, R. A. S.; Longo, R. L.; Malta, O. L.; Carlos, L. D. Photo-Click Chemistry to Design Highly Efficient Lanthanide beta-Diketonate Complexes Stable under UV Irradiation. *Chem. Mater.* **2013**, *25*, 586–598.
- (24) Asano, T.; Okada, T. Thermal Z-E Isomerization of Azobenzenes - the Pressure, Solvent, and Substituent Effects. *J. Org. Chem.* **1984**, *49*, 4387–4391.
- (25) Gao, B.; Chen, L.; Chen, T. Effect of Electron-Donating Substituent Groups on Aromatic Ring on Photoluminescence Properties of Complexes of Benzoic Acid-functionalized Polysulfone with Eu(III) ions. *Phys. Chem. Chem. Phys.* **2015**, *17*, 25322–25332.
- (26) Sun, Q.; Yan, P.; Niu, W.; Chu, W.; Yao, X.; An, G.; Li, G. NIR Luminescence of a Series of Benzoyltrifluoroacetone Erbium Complexes. *RSC Adv.* **2015**, *5*, 65856–65861.
- (27) Li, H. F.; Yan, P. F.; Chen, P.; Wang, Y.; Xu, H.; Li, G. M. Highly Luminescent Bis-diketonate Lanthanide Complexes with Triple-stranded Dinuclear Structure. *Dalton Trans.* **2012**, *41*, 900–907.
- (28) Brouwer, A. M. Standards for Photoluminescence Quantum Yield Measurements in Solution (IUPAC Technical Report). *Pure Appl. Chem.* **2011**, *83*, 2213–2228.
- (29) Frisch, M. J.; Trucks, G. W.; Schlegel, H. B.; Scuseria, G. E.; Robb, M. A.; Cheeseman, J. R.; Scalmani, G. B. V.; Mennucci, B.; Petersson, G. A.; Nakatsuji, H.; Caricato, M.; Li, X.; Hratchian, H. P.; Izmaylov, A. F.; Bloino, J.; Zheng, G.; Sonnenberg, J. L.; Hada, M.; Ehara, M.; Toyota, K.; Fukuda, R.; Hasegawa, J.; Ishida, M.; Nakajima, T.; Honda, Y.; Kitao, O.; Nakai, H.; Vreven, T.; Montgomery, J. A.; Peralta, J. E.; Ogliaro, F.; Bearpark, M.; Heyd, J. J.; Brothers, E.; Kudin, K. N.; Staroverov, V. N.; Kobayashi, R.; Normand, J.; Raghavachari, K.; Rendell, A.; Burant, J. C.; Iyengar, S. S.; Tomasi, J.; Cossi, M.; Rega, N.; Millam, N. J.; Klene, M.; Knox, J. E.; Cross, J. B.; Bakken, V.; Adamo, C.; Jaramillo, J.; Gomperts, R.; Stratmann, R. E.; Yazyev, O.; Austin, A. J.; Cammi, R.; Pomelli, C.; Ochterski, J. W.; Martin, R. L.; Morokuma, K.; Zakrzewski, V. G.; Voth, G. A.; Salvador, P.; Dannenberg, J. J.; Dapprich, S.; Daniels, A. D.; Farkas, Ö;

Foresman, J. B.; Ortiz, J. V.; Cioslowski, J.; Fox, D. J. *Gaussian 09*, Revision D.01; Gaussian, Inc.: Wallingford, CT, 2009.

(30) Saltiel, J.; Zhang, Y. X.; Sears, D. F. Temperature Dependence of the Photoisomerization of *cis*-1-(2-anthryl)-2-phenylethene. Conformer-specificity, Torsional Energetics and Mechanism. *J. Am. Chem. Soc.* **1997**, *119*, 11202–11210.

(31) Yutaka, T.; Kurihara, M.; Kubo, K.; Nishihara, H. Novel Photoisomerization Behavior of Rh Binuclear Complexes Involving an Azobenzene-bridged Bis(terpyridine) Ligand. Strong Effects of Counterion and Solvent and the Induction of Redox Potential Shift. *Inorg. Chem.* **2000**, *39*, 3438–3439.

(32) Sheldrick, G. M. SHELXT - Integrated Space-group and Crystal-structure Determination. *Acta Crystallogr., Sect. A: Found. Adv.* **2015**, *71*, 3–8.

(33) Lin, Y. J.; Zou, F.; Wan, S. G.; Ouyang, J.; Lin, L. R.; Zhang, H. Dynamic Chiral-at-metal Stability of Tetrakis(d/l-hfc)Ln(III) Complexes Capped with an Alkali Metal Cation in Solution. *Dalton Trans.* **2012**, *41*, 6696–6706.

(34) Gajda, K.; Zarychta, B.; Daszkiewicz, Z.; Domanski, A. A.; Ejsmont, K. Substituent Effects in *trans*-p, p'-Disubstituted Azobenzenes: X-ray Structures at 100 K and DFT-calculated Structures. *Acta Crystallogr., Sect. C: Struct. Chem.* **2014**, *70*, 575–578.

(35) Lednev, I. K.; Ye, T. Q.; Abbott, L. C.; Hester, R. E.; Moore, J. N. Photoisomerization of a Capped Azobenzene in Solution Probed by Ultrafast Time-Resolved Electronic Absorption Spectroscopy. *J. Phys. Chem. A* **1998**, *102*, 9161–9166.

(36) Gegiou, D.; Muszkat, K. A.; Fischer, E. Temperature Dependence of Photoisomerization. V. The Effect of Substituents on the Photoisomerization of Stilbenes and Azobenzenes. *J. Am. Chem. Soc.* **1968**, *90*, 3907–3918.

(37) Souza, B. S.; Brandao, T. A. S.; Orth, E. S.; Roma, A. C.; Longo, R. L.; Bunton, C. A.; Nome, F. Hydrolysis of 8-Quinolyl Phosphate Monoester: Kinetic and Theoretical Studies of the Effect of Lanthanide Ions. *J. Org. Chem.* **2009**, *74*, 1042–1053.

(38) Barrett, C.; Natansohn, A.; Rochon, P. *Cis-Trans* Thermal-Isomerization Rates of Bound and Doped Azobenzenes in a Series of Polymers. *Chem. Mater.* **1995**, *7*, 899–903.

(39) Wang, R. B.; Knoll, H. Rate Constants of the Thermal *cis-trans* Isomerization of Azo Dyes as Kinetic Probes in Aqueous Solutions of Poly(ethylene glycols) and Poly(ethylene oxide)-poly(propylene oxide)-poly(ethylene oxide) Block Copolymer F88. *Langmuir* **2001**, *17*, 2907–2912.

(40) Sakamoto, R.; Kume, S.; Sugimoto, M.; Nishihara, H. *trans-cis* Photoisomerization of Azobenzene-Conjugated Dithiolato-Bipyridine Platinum(II) Complexes: Extension of Photoresponse to Longer Wavelengths and Photocontrollable Tristability. *Chem. - Eur. J.* **2009**, *15*, 1429–1439.

(41) Schanze, K. S.; Mattox, T. F.; Whitten, D. G. Solvent Effects Upon the Thermal *Cis-Trans* Isomerization and Charge-Transfer Absorption of "4-(Diethylamino)-4'-Nitroazobenzene. *J. Org. Chem.* **1983**, *48*, 2808–2813.

(42) Li, J.; Li, H.; Yan, P.; Chen, P.; Hou, G.; Li, G. Synthesis, Crystal Structure, and Luminescent Properties of 2-(2,2,2-trifluoroethyl)-1-Indone Lanthanide Complexes. *Inorg. Chem.* **2012**, *51*, 5050–5057.

(43) Chen, X. Y.; Yang, X.; Holliday, B. J. Metal-Controlled Assembly of Near-infrared-emitting Pentanuclear Lanthanide Beta-diketone Clusters. *Inorg. Chem.* **2010**, *49*, 2583–2585.

(44) Binneemans, K. Lanthanide-based Luminescent Hybrid Materials. *Chem. Rev.* **2009**, *109*, 4283–4374.

(45) Shi, J.; Hou, Y.; Chu, W.; Shi, X.; Gu, H.; Wang, B.; Sun, Z. Crystal Structure and Highly Luminescent Properties Studies of Bis-beta-diketonate Lanthanide Complexes. *Inorg. Chem.* **2013**, *52*, 5013–5022.

(46) Martins, J. P.; Martin-Ramos, P.; Coya, C.; Alvarez, A. L.; Pereira, L. C.; Diaz, R.; Martin-Gil, J.; Silva, M. R. Lanthanide Tetrakis-beta-diketonate Ddimers for Solution-processed OLEDs. *Mater. Chem. Phys.* **2014**, *147*, 1157–1164.

(47) Lannes, A.; Intissar, M.; Suffren, Y.; Reber, C.; Luneau, D. Terbium(III) and Yttrium(III) Complexes with Pyridine-substituted

Nitronyl Nitroxide Radical and Different Beta-diketonate Ligands. Crystal Structures and Magnetic and Luminescence Properties. *Inorg. Chem.* **2014**, *53*, 9548–9560.

(48) Mahajan, R. K.; Kaur, I.; Kaur, R.; Uchida, S.; Onimaru, A.; Shinoda, S.; Tsukube, H. Anion Receptor Functions of Lanthanide Tris(beta-diketonate) Complexes: Naked-eye Detection and Ion-selective Electrode Determination of Cl⁻ Anion. *Chem. Commun.* **2003**, 2238–2239.

(49) Sun, J.; Song, B.; Ye, Z.; Yuan, J. Mitochondria Targetable Time-Gated Luminescence Probe for Singlet Oxygen Based on a beta-Diketonate-Europium Complex. *Inorg. Chem.* **2015**, *54*, 11660–11668.

(50) Roche, A. J.; Rabinowitz, S. A.; Cox, K. A. Efficient NMR Enantiodiscrimination of Bridge Fluorinated Paracyclophanes using Lanthanide tris Beta-diketonate Complexes. *Tetrahedron: Asymmetry* **2013**, *24*, 1382–1388.

(51) Valore, A.; Cariati, E.; Righetto, S.; Roberto, D.; Tessore, F.; Ugo, R.; Fragala, I. L.; Fragala, M. E.; Malandrino, G.; De Angelis, F.; Belpassi, L.; Ledoux-Rak, I.; Thi, K. H.; Zyss, J. Fluorinated beta-Diketonate Diglyme Lanthanide Complexes as New Second-Order Nonlinear Optical Chromophores: The Role of f Electrons in the Dipolar and Octupolar Contribution to Quadratic Hyperpolarizability. *J. Am. Chem. Soc.* **2010**, *132*, 4966–4970.

(52) Bunzli, J. C. G. Lanthanide Luminescence for Biomedical Analyses and Imaging. *Chem. Rev.* **2010**, *110*, 2729–2755.

(53) Sato, S.; Wada, M. Relations between Intramolecular Energy Transfer Efficiencies and Triplet State Energies in Rare Earth β -diketonate Chelates. *Bull. Chem. Soc. Jpn.* **1970**, *43*, 1955–1962.

(54) Aime, S.; Botta, I. M.; Fedeli, F.; Gianolio, E.; Terreno, E.; Anelli, P. High-Relaxivity Contrast Agents for Magnetic Resonance Imaging Based on Multisite Interactions Between a Beta-cyclodextrin Oligomer and Suitably Functionalized Gd(III) Chelates. *Chem. - Eur. J.* **2001**, *7*, 5261–5269.

(55) Mondal, A. K.; Jena, H. S.; Malviya, A.; Konar, S. Lanthanide-Directed Fabrication of Four Tetranuclear Quadruple Stranded Helicates Showing Magnetic Refrigeration and Slow Magnetic Relaxation. *Inorg. Chem.* **2016**, *55*, 5237–5244.

(56) Liu, S. J.; Zhao, J. P.; Tao, J.; Jia, J. M.; Han, S. D.; Li, Y.; Chen, Y. C.; Bu, X. H. An Unprecedented Decanuclear Gd(III) Cluster for Magnetic Refrigeration. *Inorg. Chem.* **2013**, *52*, 9163–9165.

(57) Regueiro-Figueroa, M.; Gunduz, S.; Patinec, V.; Logothetis, N. K.; Esteban-Gomez, D.; Tripier, R.; Angelovski, G.; Platas-Iglesias, C. Gd(3+)-Based Magnetic Resonance Imaging Contrast Agent Responsive to Zn(2+). *Inorg. Chem.* **2015**, *54*, 10342–10350.

(58) Banerjee, S. R.; Ngen, E. J.; Rotz, M. W.; Kakkad, S.; Lisok, A.; Pracitto, R.; Pullambhatla, M.; Chen, Z.; Shah, T.; Artemov, D.; Meade, T. J.; Bhujwalla, Z. M.; Pomper, M. G. Synthesis and Evaluation of Gd(III)-Based Magnetic Resonance Contrast Agents for Molecular Imaging of Prostate-Specific Membrane Antigen. *Angew. Chem., Int. Ed.* **2015**, *54*, 10778–10782.

(59) Shen, C.; New, E. J. Promising strategies for Gd-based responsive magnetic resonance imaging contrast agents. *Curr. Opin. Chem. Biol.* **2013**, *17*, 158–166.

(60) Feng, X.; Wang, L.-Y.; Wang, J.-G.; Xie, C.-Z.; Zhao, J.-S.; Sun, Q. A Unique Example of a 3D Framework Based on the Binuclear Dysprosium(III) Azobenzene-3,5,4'-tricarboxylate with 3,6-Connected Topology Showing Ferromagnetic Properties. *CrystEngComm* **2010**, *12*, 3476–3478.

(61) Biswas, S.; Jena, H. S.; Sanda, S.; Konar, S. Proton-Conducting Magnetic Coordination Polymers. *Chem. - Eur. J.* **2015**, *21*, 13793–13801.

(62) Chandrasekhar, V.; Das, S.; Dey, A.; Hossain, S.; Sutter, J. P. Tetranuclear Lanthanide(III) Complexes Containing Dimeric Subunits: Single-molecule Magnet Behavior for the Dy₄ analogue. *Inorg. Chem.* **2013**, *52*, 11956–11965.

(63) Biswas, S.; Adhikary, A.; Goswami, S.; Konar, S. Observation of a Large Magnetocaloric Effect in a 2D Gd(III)-based Coordination Polymer. *Dalton Trans.* **2013**, *42*, 13331–13334.